# IMPROVEMENT OF ENERGY MANAGEMENT SYSTEM FOR MAXIMUM BATTERY RELIABILITY IN STANDALONE PHOTOVOLTAIC APPLICATIONS

**Raja YAHMADI**
Research Laboratory Materials, Measurements and Applications, National Institute of Applied Science and Technology (INSAT), (+216) 71 704 329, Tunis
yahmadiraja@gmail.com

**Kais BRIK**
Institute of Multimedia Arts of Manouba (ISAMM), Tunis
kais.brik@yahoo.fr

**Faouzi BEN AMMAR**
Research Laboratory Materials, Measurements and Applications, National Institute of Applied Science and Technology (INSAT), (+216) 71 704 329, Tunis
faouzi.benamar@insat.rnu.tn

***Abstract:*** *This paper aims to ensure the Maximum Battery Reliability (MBR) in the standalone photovoltaic (PV) application by improving the Energy Management System (EMS). In fact, the intermittent nature of PV energy and the unsuitable charge control strategy cause the lead acid battery degradation by the electrolyte stratification, the non-cohesion of active mass, the corrosion and the hard sulfating of the electrodes. In this context, a qualitative analysis of the battery performances under the conventional charge control strategies is presented. Then, the authors propose an advanced charge control strategy based on the multistep current profile in order to avoid the degradation phenomena of battery and increase its reliability. The experimental result shows that the proposed charge control strategy avoids the corrosion phenomenon and the non-cohesion of active mass caused by the overcharge and the hard sulfating phenomenon and the electrolyte stratification generated by the incomplete charge. Finally, an improvement of EMS by properly incorporating the advanced charge control strategy is archived and discussed. The results show that the proposed EMS ensures the maximum battery reliability and preserves its capacity in the standalone PV application.*

***Key words:*** *Batteries, Degradation, Energy management, Photovoltaic systems, Reliability.*

## 1. Introduction

In the standalone photovoltaic system, the use of energy storage system such as the lead acid battery is required to ensure the continuity of energy [1]. However, the operating conditions of battery in this application generate the decreasing of its performances and lifetime [2-4]. In this context, the improvement of the lead acid battery lifetime is ensured by the integration of an adequate energy management system which allows preventing the occurrence of the failure modes. Indeed, the deep discharge which causes the electrolyte stratification and the hard sulfating of the electrode is avoided by limiting the maximum level of discharge to 50% [5-7]. The overcharge and incomplete charge are avoided by developing a more appropriate charge control strategy. Recently, the research community has shown considerable interest in the charge control strategies of battery in the PV application. Among the most common charge control strategies, there are the control strategy based on the maximum state of charge and that based on the maximum voltage [8,9]. During the charge control strategy based on the maximum state of charge, the battery is disconnected when its state of charge reaches 100% of rated capacity [8]. For the charge control strategy based on the maximum voltage, the charging of the battery is stopped when its voltage reaches the maximum voltage. However, these conventional charge control strategies do not ensure the maximum battery reliability. The main objective of this paper is to improve the energy management system for ensures the maximum battery reliability in the standalone PV application by integrating a suitable control strategy.

The improvement strategy of battery reliability is based on two stages.

In the first stage, a topology description of the photovoltaic system is firstly presented. Then, a study of MPPT algorithm for photovoltaic generator is presented. An experimental investigation of the conventional charge control strategies is carried out to identify the critical degradation modes of battery and their causes.

In the second stage, the avoiding of the battery degradation is performed by the development of the advanced charge control strategy. This advanced charge control strategy is based on the multistep current profile, where the regulation of current depends to the battery voltage and state of charge. The experimental investigation of the advanced charge control strategy is carried out. Finally, the improvement of energy management system by integration of the advanced charge control strategy is presented and validated using simulation data.

## 2. Conventional energy management system

### A. Topology description of standalone photovoltaic system

In the PV system, the PV array is composed of several modules connected in series and parallel to form an appropriate output power. An adaptation stage between the PV array and the DC bus is provided by a DC-DC buck converter. This adaptation stage is controlled by a Maximum Power Point Tracking (MPPT) algorithm that presents oscillations around the Maximum Power Point (MPP) of the PV array in any weather condition (solar irradiance, temperature). The batteries are connected also to the PV system in order to ensure a continuous availability of energy [10,11]. A bidirectional DC–DC converter is connected between the DC bus and the batteries to provide the charging and discharging mode of the battery packs. In the photovoltaic system, the development of energy management system is required to effectively manage the flow of energy between the different elements of the system [12-17].
Figure 1 shows the topology of standalone photovoltaic system.

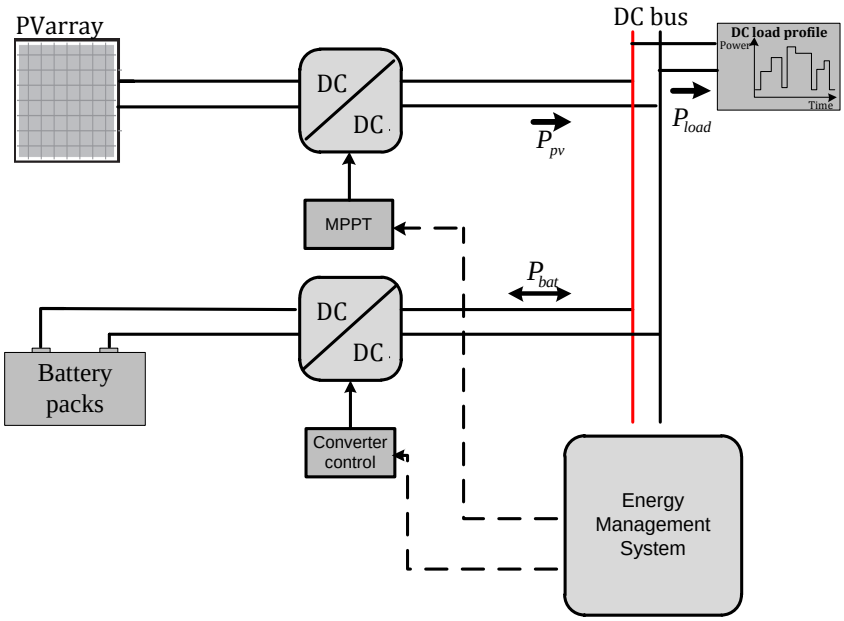


Fig 1. Topology of standalone photovoltaic system.

The conventional energy management algorithm is illustrated in Fig.2. Firstly, the system parameters are measured (photovoltaic current $I_{pv}$, load current $I_{load}$, photovoltaic voltage $V_{pv}$, load voltage $V_{load}$, battery packs voltage $V_{batp}$ and state of charge SOC) to calculate the difference between the produced power by the PV array ($P_{PV}$) and the demanded power by the load ($P_{load}$). This difference allows controlling the distribution of energy in the system. Indeed, the EMS operation can be divided in three cases.

The first case is archived when the produced power by the PV array is equal to the demanded power by the load ($P_{pv}=P_{load}$). In this case, the demanded power by the load is totally supplied by the PV array.

$$P_{load} = P_{pv} \quad (1)$$

The second case occurs when the PV power is insufficient to supply the load ($P_{pv}<P_{load}$). In this case, an evaluation of the battery state of charge is achieved and two main sub-cases are observed.
-When the battery state of charge is higher than the minimum state of charge ($SOC \geq SOC_{min}=50\%$), the load is supplied by the battery packs and the PV array. The demanded power of load is expressed as:

$$P_{load} = P_{pv} + P_{batp} \quad (2)$$

If the battery state of charge is less than the minimum state of charge ($SOC < SOC_{min} = 50\%$), the battery packs and the load are disconnected.

$$P_{load} = 0 \quad (3)$$

The third case is shown when the generated power from the PV array is greater than the demanded power by the load ($P_{pv}>P_{load}$). In this case, the battery packs is charged according to the conventional charge control strategies. These conventional charge control strategies are based on the maximum state of charge or the maximum voltage. The battery packs are charged by the current $I_{pv}$-$I_{load}$ and the absorbed power by the load is expressed as follows:

$$P_{load} = P_{pv} - P_{batp} \quad (4)$$

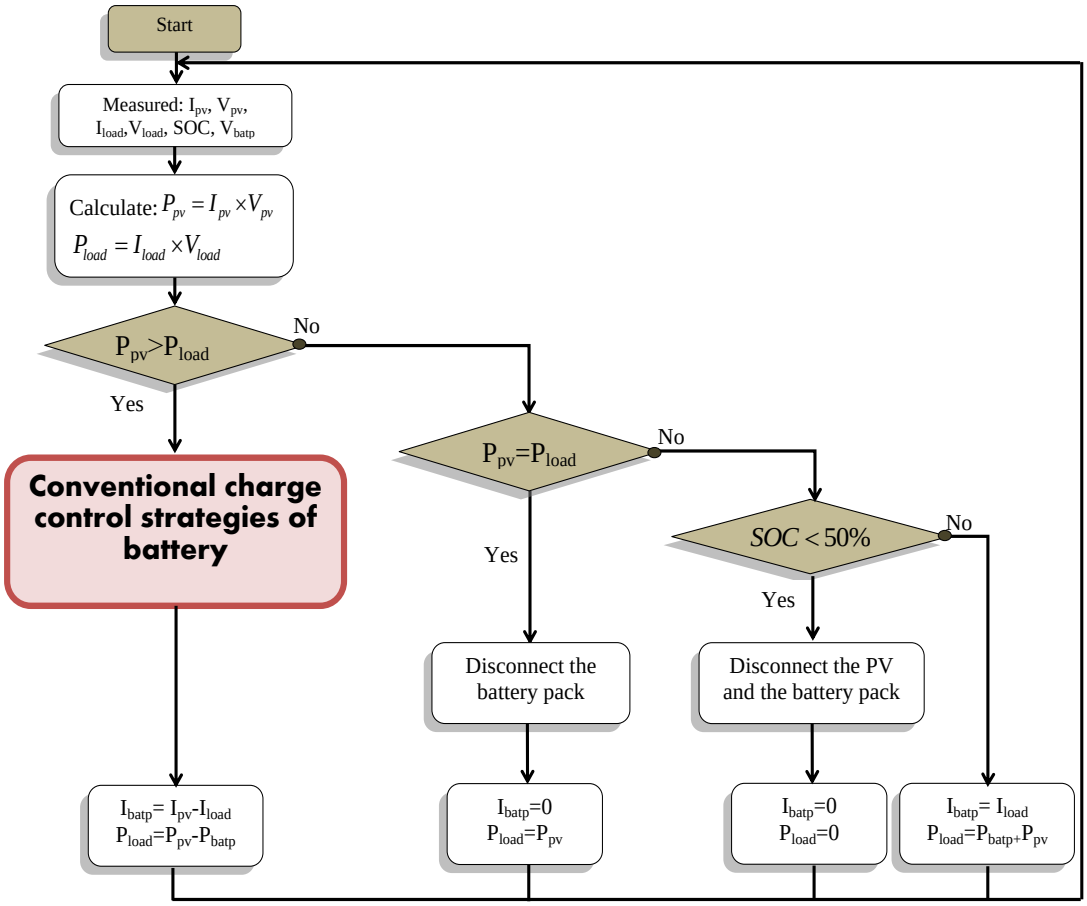


Fig 2. Conventional energy management algorithm.

The energy management in the standalone photovoltaic system based on the conventional charge strategies of the battery generates its degradation and not ensure its optimum reliability [18, 19]. Therefore, the compatibility between battery requirements and the associated charge control strategy seems to be a critical point to extend its lifetime. By analyzing the effect of the conventional charge control strategy on battery reliability, the results allow to provide technical recommendations for a suitable charge control strategy. In this context, the MPPT algorithm for the DC–DC buck converter and the conventional charge control strategies for the bidirectional DC– DC converter used in the standalone photovoltaic system are explained as follows.

### B. MPPT Algorithm For DC-DC buck converter

In standalone photovoltaic system, the DC–DC buck converter performs the MPPT function or limiting power depending on the battery state of charge. Therefore, the battery state of charge is sent and used to control the controllable switch. When the battery state of charge SOC is lower than 100%, the DC–DC buck converter performs the MPPT function. The output voltage $V_{pv}$ an output current $I_{pv}$ of the photovoltaic generator are detected and sent to the MPPT function in order to drive the converter switch by the duty cycle variation[20]. In addition, the buck converter limits the power generated by the PV generator when the battery state of charge is equal to 100%. In this case, the limiting power controller restricts the output power of PV generator in order to protect the battery packs from the overcharging. Figure 3 shows the DC-DC buck converter with control blocks diagram.

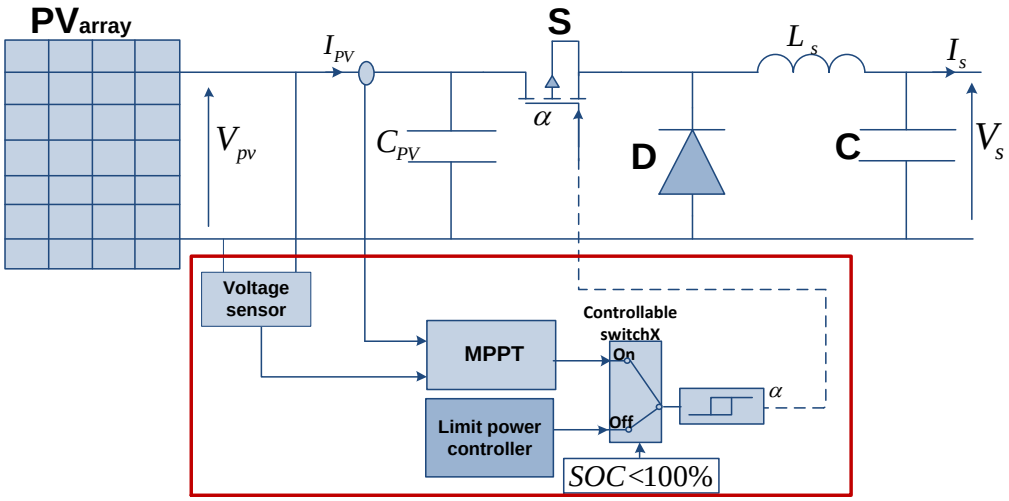


Fig 3. Buck converter with control blocks diagram.

The most common algorithms are: Hill Climbing, Perturb and Observe (P&O) and Increment conductance (IncCond). The Hill-climbing and P&O algorithms have the same disadvantages about the oscillations around the MPP and the occasional loss to research the MPP during the fast changing of weather conditions. The MPPT algorithm proposed is the IncCond algorithm due to its high performance compared to the other algorithms. In fact, this algorithm offers the advantage of providing high efficiency under the fast changing of weather conditions [21-23].

The principle of IncCond is based on the following conditions [24]:

- If $dV_{pv}=0$ and $dI_{pv}=0$, the operating point of PV array corresponds to MPP and the previous value of duty cycle is maintained.
- If $dV_{pv}=0$ and $dI_{pv}>0$, the MPPT should increase the duty cycle value in order to track the MPP.
- Otherwise, if $dI_{pv}<0$, the MPPT should decrease the duty cycle value.

With:

$$dI_{pv}(k) = I_{pv}(k) - I_{pv}(k-1) \quad (5)$$

$$dV_{pv}(k) = V_{pv}(k) - V_{pv}(k-1) \quad (6)$$

- If $dV_{pv}\neq 0$, the IncCond algorithm is based on the cancellation of the power derivative relative to the voltage derivative, as described in the following equations:

$$\frac{dP_{pv}}{dV_{pv}} = I_{pv} \times \frac{dV_{pv}}{dV_{pv}} + V_{pv} \times \frac{dI_{pv}}{dV_{pv}} = I_{pv} + V_{pv} \times \frac{dI_{pv}}{dV_{pv}} = 0 \quad (7)$$

$$-\frac{I_{pv}}{V_{pv}} = \frac{dI_{pv}}{dV_{pv}} \quad (8)$$

The equality of the equation (8) indicates that MPPT is still operating at the MPP and the previous value of duty cycle is maintained. The inequality of this equation indicates the position of the operating point by comparing at each instant:

- $$\frac{dI_{pv}}{dV_{pv}} > -\frac{I_{pv}}{V_{pv}}, (\frac{dP_{pv}}{dV_{pv}} > 0) \quad (9)$$

In this case, the operating point of the PV array is on the left of MPP and the duty cycle value should increase.

- $$\frac{dI_{pv}}{dV_{pv}} < -\frac{I_{pv}}{V_{pv}}, (\frac{dP_{pv}}{dV_{pv}} < 0) \quad (10)$$

The operating point of the PV array is on the right of MPP and the duty cycle value is decreased.

Table I lists the electrical characteristics of the PHOTOWATT module specified at Standard Testing Conditions STC (An irradiance of 1000W/m$^2$ and a temperature of 25°C).

Table I.

Electrical characteristics of PHOTOWATT PV module.

| Parameters | Value |
|---|---|
| Maximum power | 250W |
| Voltage at maximum power | 30.7V |
| Current at maximum power | 8.15A |
| Short circuit current | 8.63A |
| Open circuit voltage | 37.4V |

Figure 4 shows the voltage, current and power at the output and input of the DC-DC buck converter under STC. The PV generator consists of 4 PV modules connected in parallel.

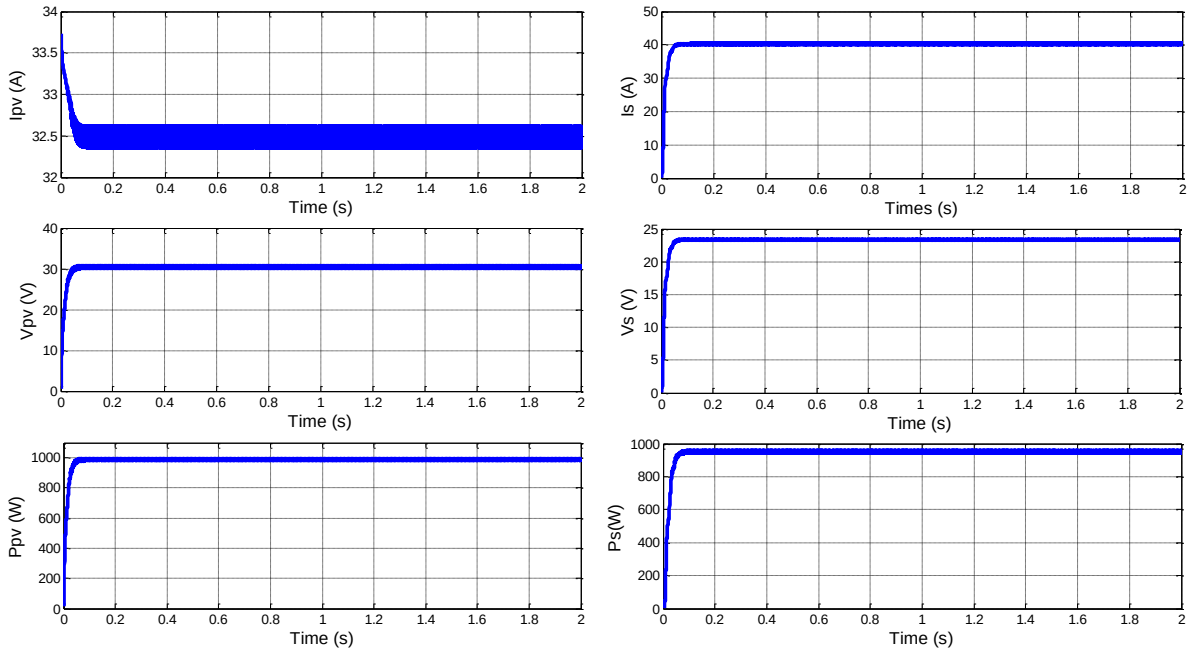


Fig 4. Voltage, current and power at the output and input of the Buck converter.

As seen in Figure 4, the MPPT control oscillates the operating point around the MPP point. At the output of the PV array, the voltage and current stabilize respectively around 30.4V and 32.5A. At the output of the DC-DC buck converter, the voltage and current respectively stabilize around 24V and 39.6A. It shows also that the output power of the PV array stabilizes around 989W and the output of the DC-DC buck converter stabilizes around 950W. Therefore, a loss of power around 39W is presented due to the switching and conduction losses in the MOSFET transistor, diode and the various components of the MPPT control. These results show that the DC-DC buck converter and the MPPT control are correctly performs their roles.

### C. Conventional charge control strategies of battery

The most common charge control strategies of battery are based on the maximum state of charge or the maximum voltage [23]. Fig. 5 presents the conventional charge control strategies.

When the power required by the load is greater than that supplied by the primary source, the battery ensures the continuity of service and provides the additional power required. In this case, the battery is disconnected when its state of charge SOC reaches 50% in order to avoid the deep discharge. When the source power is greater than the load power, the battery is charged until it is fully charged. During the charge control strategy based on the maximum state of charge, the battery is disconnected when its state of charge reaches 100% of rated capacity. For the control strategy based on the maximum voltage, the battery is disconnected when its voltage reaches the maximum voltage $V_{bat\text{-}max}$. In these control strategies, the hysteresis comparator is used to compare the reference current $I_{ref}$ with the battery charging current $I_{bat}$. The output of this comparator generates a duty cycle which indicates the switching periods of the converter switches.

The battery state of charge (SOC) % is determined by equation 7.

$$SOC\% = SOC_{ini}\% + \int_0^t \frac{I_{bat}(t)\times dt}{C}\times 100 \tag{11}$$

With: C is the nominal capacity; $SOC_{ini}$ is the initial SOC (%)

The maximum voltage is determined by the following equation:

$$V_{bat-\max} = Number\ of\ cell \times 2.4 - 0.005\times(T-25) \tag{12}$$

With:

T: Ambient temperature.

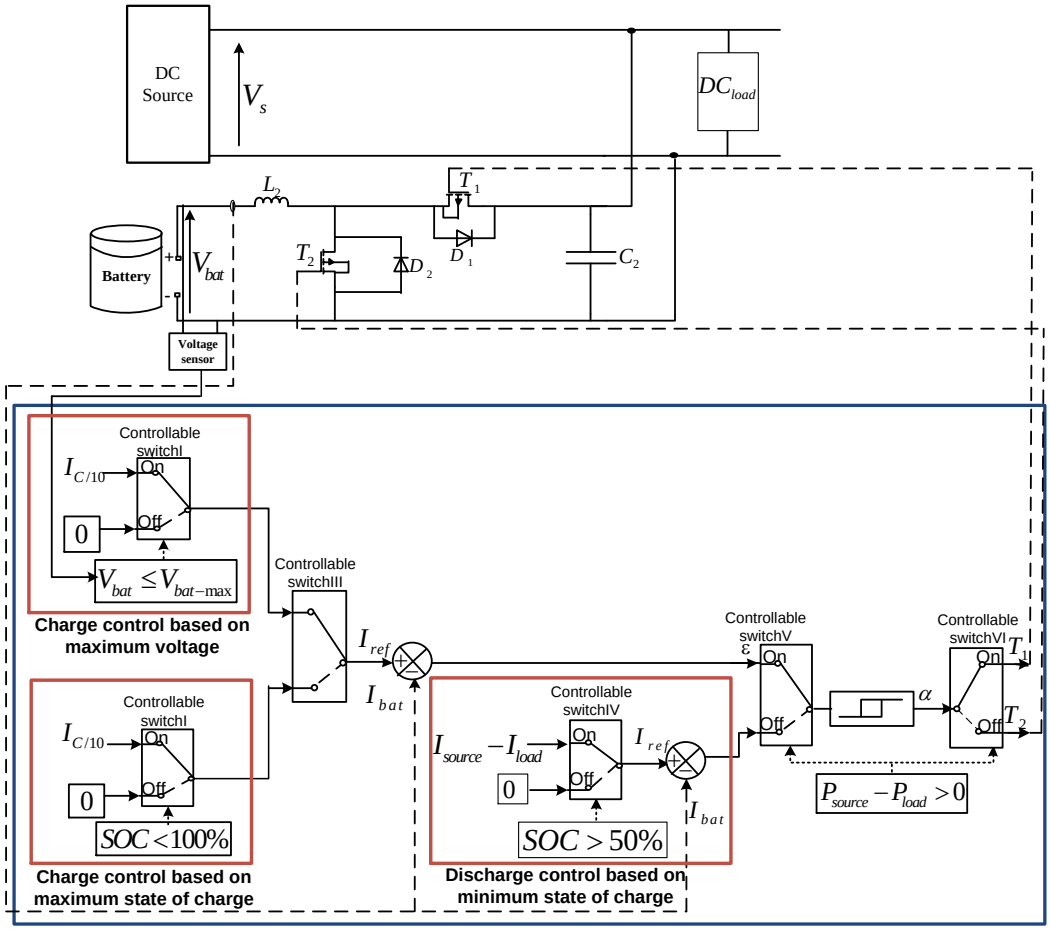


Fig 5. Charge control strategies of lead acid battery.

The qualitative analysis of the lead acid battery characteristic under the conventional charge control strategies is performed by an experimental measurement of a lead acid battery characteristic that has a rated voltage of 12V and a rated capacity of C=90Ah.

The experimental and simulation result of the current, voltage and state of charge during the battery charging mode with initial state of charge $SOC_{ini}$=60% is presented in Fig.6.

As shown in Fig. 6, the simulation results are in good agreement with the measured values. During the charging mode, the state of charge and the voltage of the battery increase in a linear way until reaching theirs maximal value. The results of the charge control strategy based on the maximum state of charge (Fig.6 a) show that when the state of charge reaches 100%, the battery voltage exceeds the maximum voltage (14.95V>$V_{bat-max}$=14.4V) which causes the overcharge. This overcharge generates the gassing phenomenon during 34min which can loosen the active mass into the plates. This gassing phenomenon is accompanied by a decrease in the level of electrolyte which leads the electrodes in contact with the air and generates the corrosion of the electrodes [25].

The results of the charge control strategy based on the maximum voltage (Fig.6 b) show that when the battery voltage reaches $V_{bat-max}$, the state of charge SOC is less than 100%. The battery is then in an incomplete state of charge which causes the growth of the sulfate crystals and generates the irreversible formation of lead sulfate in the active mass. Over time, the hard sulfating phenomenon is appeared on the electrode and accelerated the battery ageing. Similarly, the incomplete charge does not ensure the homogenization of the electrolyte, which facilitates the appearance of the stratification.

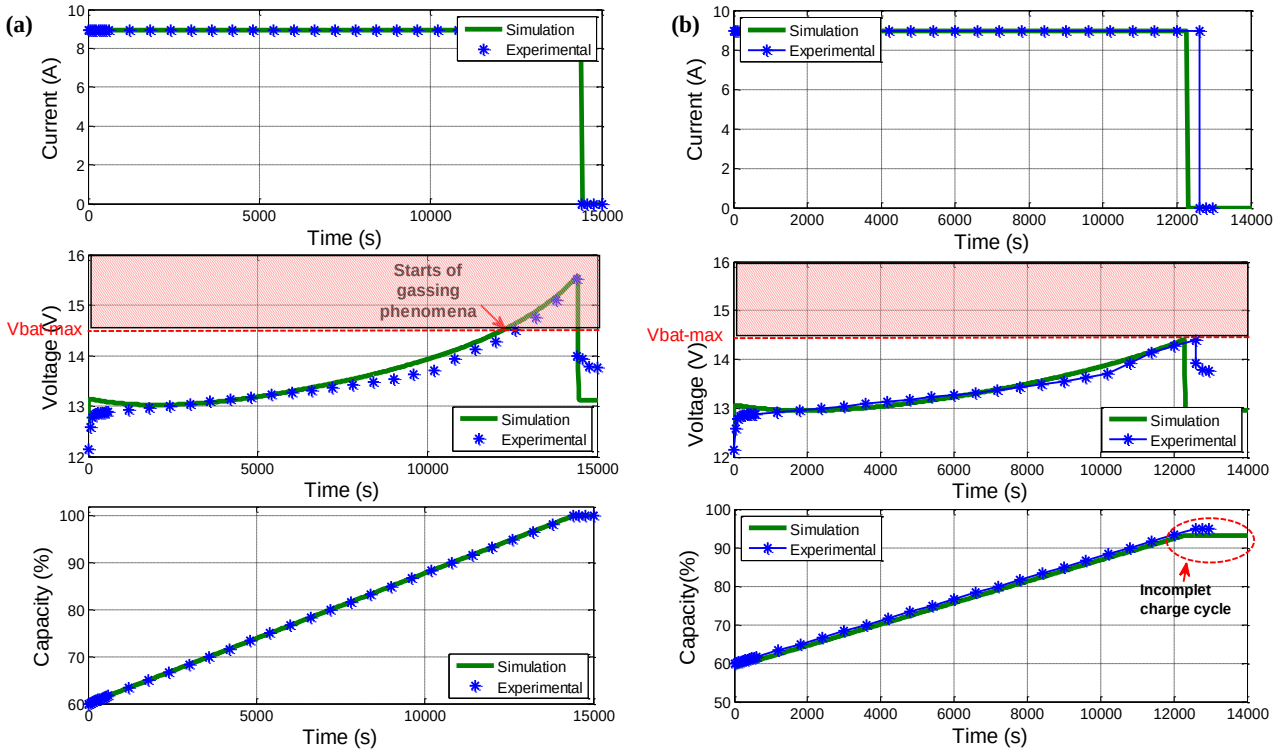


Fig 6. Current, Voltage and State of charge of the battery

This qualitative analysis allows the identification of the critical causes of the battery degradation by conventional charge control strategies. The results obtained from the two conventional charge control strategies do not allow ensuring the operation of the battery under suitable conditions. Indeed, the experimental results show that the charge control strategy based on the maximum state of charge generates the corrosion phenomenon and the non-cohesion of the active mass, whereas that based on the maximum voltage produces the hard sulfating phenomenon and the electrolyte stratification.

## 3. Improvement of energy management system

In the standalone photovoltaic applications, an improvement of the energy management system is required in order to optimally manage the charge and discharge mode of the battery. In this sense, an advanced charge control strategy should be developed in order to ensure that the charging regime is the best that can be done. Then, a study of the integration of the advanced charge control strategy in the energy management system is carried out.

### A. Advanced charge control strategy of battery

In this section, the authors propose an advanced charge control strategy based on the multistep current profile in order to prevent the appearance of aging phenomena and extend the battery lifetime. This proposed control strategy allows to reach a state of charge SOC = 100% with a battery voltage below the maximum voltage. The advances charge control strategy is given in Fig.7.

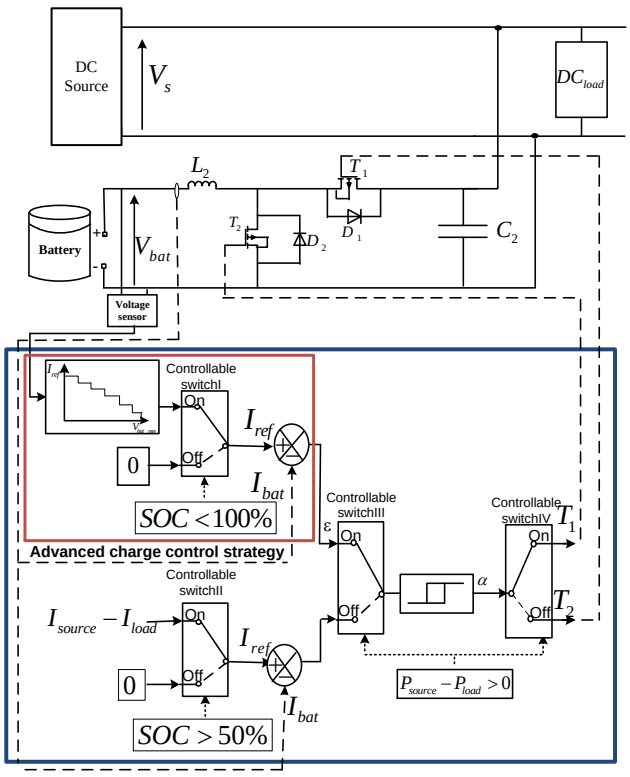


Fig 7. Advanced charge control strategy of battery.

In the stand-alone photovoltaic application, the lead-acid battery is used intensively that impose the

integration of the multistep current with n = 4 [6]. This charge control strategy is composed of two stages:

- First stage: The battery is charged with a constant current $I_{C/10}$ until the floating voltage $V_{bat\text{-}floating}=V_{step\text{-}0}$. The floating voltage is defined as:

$$V_{bat-floating} = Number\ of\ cell \times 2.27 - 0.005 \times (T - 25) \quad (13)$$

- Second stage: the battery is charged with a current that decreases progressively according to the battery voltage until the full state of charge (Table II). For the step k=1, the battery is charged by the current $I_{step\text{-}1}$ until its voltage reaches $V_{steps\text{-}1}$. If $V_{bat}=V_{step\text{-}1}$, the step k=2 is activated and the battery is charged by the current $I_{step\text{-}2}$ until its voltage reaches $V_{steps\text{-}2}$. If $V_{bat}=V_{step\text{-}k}$, k step is activated and the battery is charged by the current $I_{step\text{-}k}$ until its voltage reaches $V_{steps\text{-}k}$ [6].

The charging current $I_{step\text{-}k}$ and the voltage $V_{steps\text{-}k}$ in each step is determined by:

$$I_{step\_k} = I_{C/10} - k \times \Delta I_{bat-steps} \quad (14)$$

And

$$V_{steps\_k} = V_{bat-floating} + k \times \Delta V_{bat-steps} \quad (15)$$

$$\Delta V_{bat-steps} = \frac{V_{bat-max} - V_{bat-floating}}{4} = 0.195V \quad (16)$$

$$\Delta I_{bat-steps} = \frac{I_{C/10} - I_{C/50}}{4} = 1.8A \quad (17)$$

$I_{C/50}$ is current at the end of the charge that limits the "gassing" phenomena.

Table II.

Voltages And Currents In Each Step.

| K | 0 | 1 | 2 | 3 | 4 |
|---|---|---|---|---|---|
| $I_{steps\text{-}k}$ (A) | 9 | 7.2 | 5.4 | 3.6 | 1.8 |
| $V_{steps\text{-}k}$ (V) | 13.62 | 13.81 | 14.01 | 14.20 | 14.4 |

The results (Fig.8) show that the proposed charge control strategy based on the multistep current profile avoids the sulfating phenomenon and the stratification of the electrolyte by the full state of charge (SOC=100%). It is also noted that this maximum capacity is reached with the battery voltage lower than the maximum voltage ($14.22V<V_{bat\text{-}max}=14.4V$) which proves the elimination of the corrosion phenomenon and non-cohesion of the active masse. Therefore, the advanced charge control strategy ensures the maximum battery reliability by avoiding the appearance of the degradation phenomena.

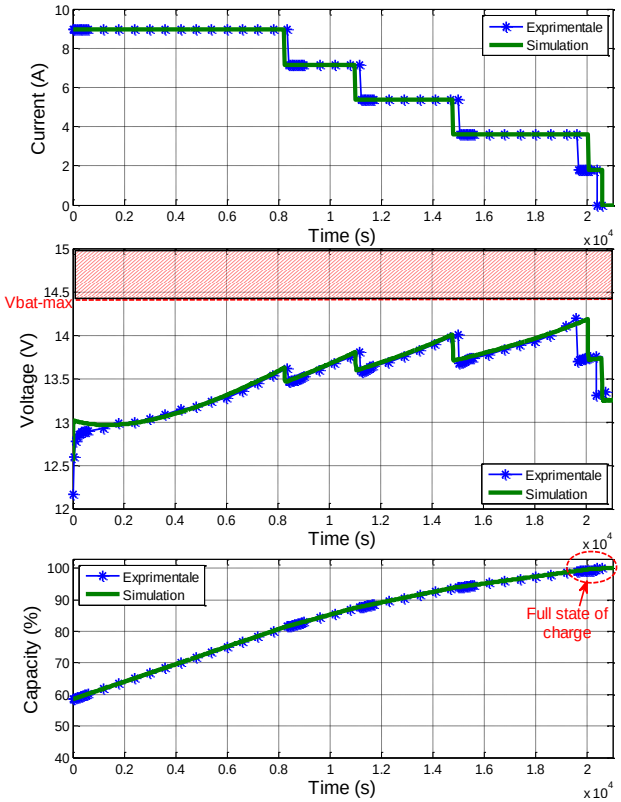


Fig.8. Current, Voltage and State of charge of the battery under the advanced charge control strategy.

## B. Results and discussion

The integration of the advanced charge control strategy of the battery in the energy management system is presented in this section to validate its efficiency for the standalone PV application. Fig.9 depicted the proposed energy management algorithm.

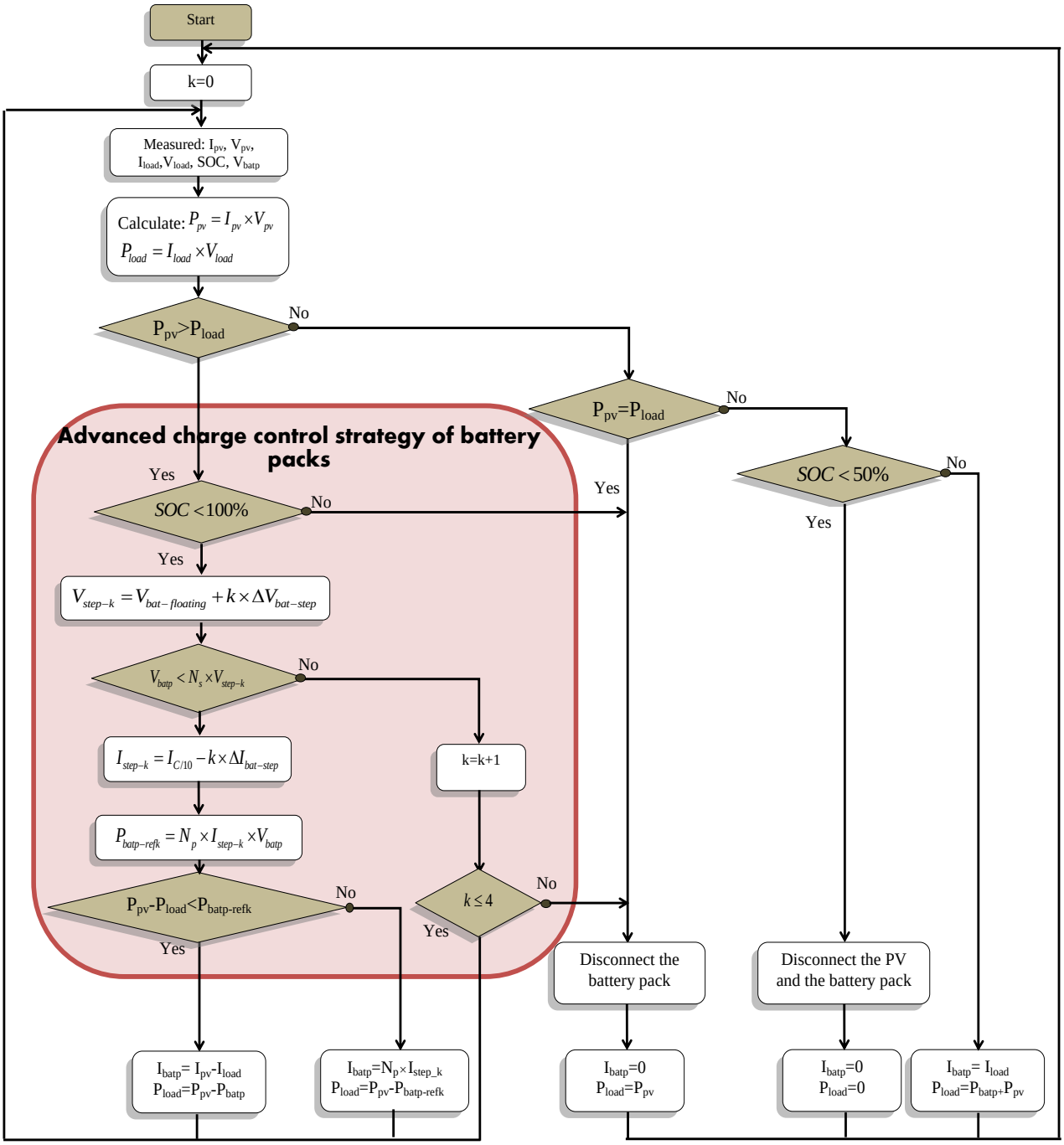


Fig 9. Proposed energy management algorithm.

Firstly, the initialization of the step k=0 is performed and the system parameters are measured to calculate the difference between $P_{PV}$ and $P_{load}$. Then, the EMS operation can be divided in three cases.

When $P_{pv}$=$P_{load}$, the demanded power by the load is totally supplied by the PV array (equation (1)).

When $P_{pv}$<$P_{load}$ and SOC≥$SOC_{min}$=50%, the load is supplied by the battery packs and the PV array (equation (2)) whereas when $P_{pv}$<$P_{load}$ but SOC <$SOC_{min}$ = 50%, the battery packs and the load are disconnected (equation (3)).

When $P_{pv}$>$P_{load}$, an evaluation of the battery state of charge is carried out and three cases occur:

- If the battery packs are fully charged (SOC=$SOC_{max}$), they are disconnected and the absorbed power by the load is expressed as:

$$P_{load} = P_{pv} \tag{18}$$

Otherwise; if the battery packs are not fully charged (SOC<$SOC_{max}$=100%), the calculation of the voltage $N_s \times V_{step\_k}$ is carried out.

-If the battery packs voltage $V_{batp}$ is lower than the voltage $N_s \times V_{step\_k}$. In this case, a calculation of $I_{step\_k}$ and an evaluation of the residual power amount are

carried out.

- If this residual power is greater than the power $P_{batp\text{-}refk}$ ($P_{pv}$-$P_{load}$>$P_{batp\text{-}refk}$), the battery packs is charged with the current $N_p \times I_{step\text{-}k}$ and the demanded power by the load is expressed as:

$$P_{load} = P_{pv} - P_{batp\_refk} \quad (19)$$

With

$$P_{batp\text{-}refk} = N_p \times I_{step\text{-}k} \times V_{batp} \quad (20)$$

- If the residual power is less than the power $P_{batp\text{-}refk}$ ($P_{pv}$-$P_{load}$<$P_{batp\text{-}refk}$), the battery packs are charged by the current $I_{pv}$-$I_{load}$ and the absorbed power by the load is expressed as follows:

$$P_{load} = P_{pv} - P_{batp} \quad (11)$$

-If $V_{batp}$ is higher than $N_s \times V_{step\_k}$, the value of k is incremented until $V_{batp}$ is lower than the new voltage $N_s \times V_{step\_k}$.

The simulation results are obtained for a photovoltaic system composed of a 1KW PV array, an average load power equal to 200W and a DC bus voltage of 24V. The sizing of the battery energy storage is determined to ensure the continuity of energy for two-day of autonomy. The storage capacity of the electrical energy depends on the required power of the load and on its autonomy; it is estimated by the following equation [26]:

$$C_{batp} = \frac{E_{load-average}\ N_a}{\eta_{bat}\ V_{batp}\ DOD} \quad (22)$$

With:

$C_{batp}$: Storage capacity of the battery packs,

$E_{load\text{-}average}$: Required average energy for load,

$N_a$: Number of autonomy days,

DOD: Deep of discharge,

$\eta_{bat}$: Battery efficiency.

Table III presents the characteristics of the battery packs as well as the limit voltages for the multi-steps current control with n = 4.

TABLE III.

Battery packs characteristics

| | |
|---|---|
| Rated voltage of battery packs $V_{batp}$ | 24V |
| Capacity of battery packs storage $C_{batp}$ | 900AH |
| Battery in parallel $N_p$ | 5 |
| Battery in series $N_s$ | 2 |
| Rated voltage of battery $V_{bat}$ | 12V |
| Capacity of battery storage $C_{bat}$ | 90AH |

Fig.10 presents the configuration of standalone photovoltaic system with batteries.

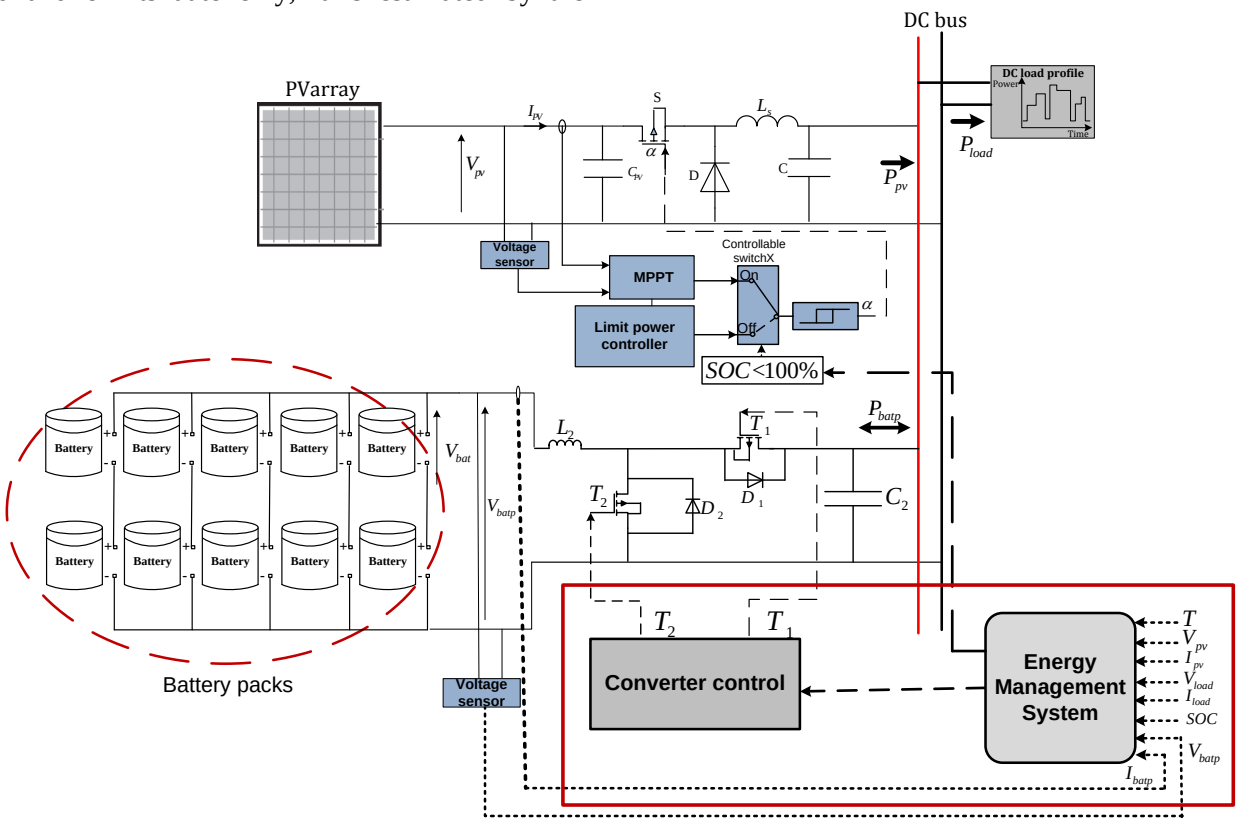


Fig 10. Configuration of standalone photovoltaic system with batteries.

The description of the energy management system function with the advanced charge control strategy is developed as follows (Figure 11).The control block diagram for the bidirectional converter is used to determine the charging or discharging mode of the battery packs.

If the $P_{pv}$ is higher than $P_{load}$, the bidirectional converter performs the charging mode of the battery packs by the control of the power electronic switch $T_1$.

- When SOC<100%, the battery packs are charged by the multi-steps current. The battery packs voltage $V_{batp}$ is sent to control the controllable switch V, IV, III, II and I.
- When $V_{batp}$ <27.24V and $P_{pv}$-$P_{load}$>$P_{batp\text{-}refk}$ , the controllable switches V and VIII are On and the reference current $I_{ref}$ is 45A.
- When 27.62V ≤ $V_{batp}$ < 27.24V and $P_{pv}$-$P_{load}$>$P_{batp\text{-}refk}$, the controllable switch V is Off while the controllable switches IV and IX are On and the reference current is 37.5A.
- When 27.62V ≤$V_{batp}$< 28.02V and $P_{pv}$-$P_{load}$>$P_{batp\text{-}refk}$, the reference current is 27A. In this case, the controllable switchIV becomes Off and the controllable switches III and X are On.
- When 28.02V ≤$V_{batp}$ < 28.4V and $P_{pv}$-$P_{load}$>$P_{batp\text{-}refk}$, the reference current is 18A where the controllable switch III is Off and the controllable switches II and XI are On.
- When 28.4V ≤$V_{batp}$ <28.8V and $P_{pv}$-$P_{load}$>$P_{batp\text{-}refk}$, the battery packs are charged by current 9A and the controllable switch II is Off while the controllable switches I and XII are On. Else if $P_{pv}$-$P_{load}$<$P_{batprefk}$ , the reference current $I_{ref}$ is $I_{pv}$-$I_{load}$ .

If the $P_{pv}$ is lower than $P_{load}$, the bidirectional converter performs the discharging mode of the battery packs by the control of the power electronic switch $T_2$ .

- When SOC > 50%, the controllable switch IX is On and the reference current $I_{ref}$ is equal to $I_{pv}$-$I_{load}$, else it is Off.

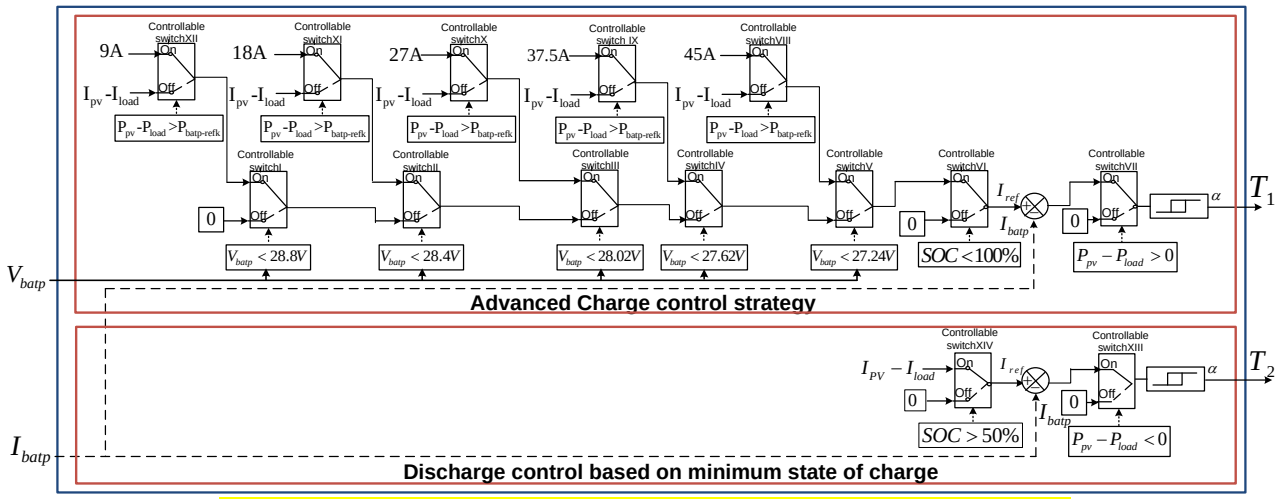


Fig 11. Circuit configuration of advanced control strategy block diagram.

Fig. 12 shows the performance of the proposed EMS with an advanced charge control strategy during a day.

The various operation modes of EMS are examined by this simulation according to the real working conditions, which includes periods of sufficient and insufficient PV output power. It shows that during the midnight period up to 5am the output power of the PV array is absent, the battery packs supplies the load ($P_{load}$ = $P_{batp}$). As soon as the sun rises, the generated power by the PV array increases progressively and the load is supplied by the PV array and the battery packs ($P_{load}$ = $P_{pv}$ + $P_{batp}$). Once the produced power by the PV array is greater than or equal to the absorbed power by the load (t = 7am), the load is supplied by the PV array and the residual power charges the battery packs. The batteries are therefore charged according to the advanced control strategy by the multistep current with n = 4. From 5pm, the output power of the PV array becomes less than that required by the load and therefore, the battery packs is discharged to supply the load. At 8pm, the PV array is unavailable, so the battery packs supplied the required load power.

The state of charge of the battery packs reaches 100% at t = 2.90pm with a voltage lower than the maximum voltage ($V_{batp}$=28.6V<$V_{batp\text{-}max}$=28.8V), thus avoiding the degradation phenomena. It is also shown that the battery state of charge is preserved between 50% and 100%, which guarantees the maximum battery reliability and extending its lifetime. Therefore the role of the energy management system in the PV system is to provide decisions on energy management between the various components of the stand-alone PV system and to protect the battery against the degradation phenomena.

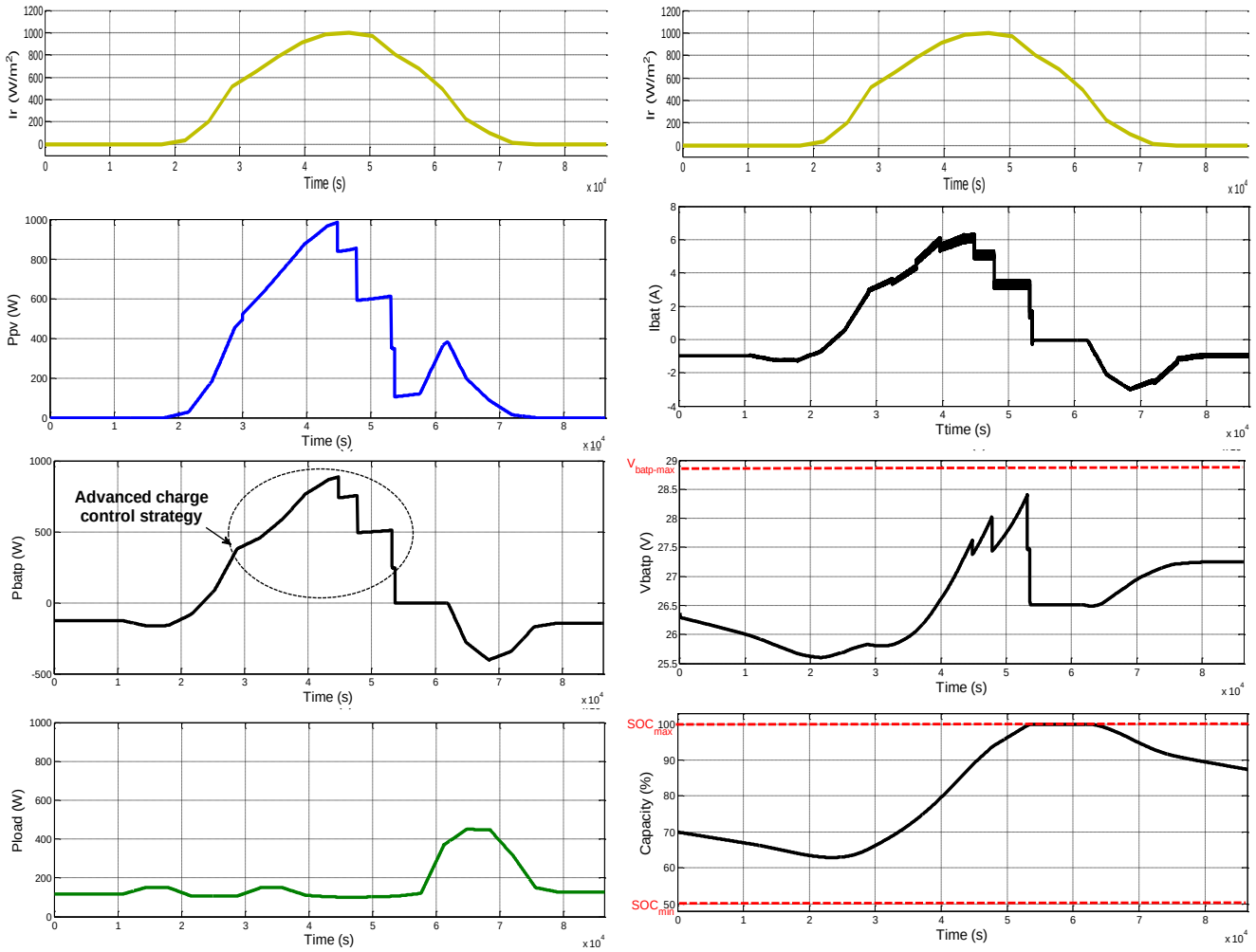


Fig.12. Performance of the proposed EMS with advanced charge control strategy during a day.

## 5. Conclusion

This paper shows that the conventional charge control strategy based on the maximum state of charge causes the appearance of the corrosion phenomenon and the non-cohesion of active mass. On the other hand, the charge control strategy based on the maximum voltage causes the sulfating of the electrodes and the electrolyte stratification. In this context, the author proposes an advanced charge control strategy to avoid the degradation phenomena of lead acid battery. The experimental results prove that the advanced charge control strategy allows to reaches the battery full state of charge SOC=100% with a terminal voltage lower than the maximum voltage that avoids the degradation phenomena. Finally, the validation of the proposed EMS with an advanced charge control strategy based on the multisteps current profile is performed using simulation data during one day. The simulation result shows the efficiency of the proposed EMS to improve the lead acid battery reliability in the standalone PV system.

## References


1. B.J. Huang, P.C. Hsu, M.S. Wu, P.Y. Ho, "*System dynamic model and charging control of lead-acid battery for stand-alone solar PV system*", Solar Energy, vol. 84, pp.822–830, 2010.
2. D. Benchetrite, M. Le Gall, O. Bach, M. Perrin, F. Mattera, "*Optimization of charge parameters for lead–acid batteries used in 3photovoltaic systems*", Journal of Power Sources, vol.144, pp. 346–351, 2005.
3. J. Xio, L. Bai, Z. Lu, K. Wang, "*Method, Implementation and application of energy storage system designing*", International transactions on electrical energy systems, vol.24, pp. 378-394, 2014.
4. H. Yang, H. Wang, G. Chen, G. Wu, "*Influence of the charge regulator strategy on state of charge and lifetime of VRLA battery in household photovoltaic systems*", Solar Energy, vol.80, pp.281–287, 2006.
5. A. Urtasun, P. Sanchis, D. Barricarte, L. Marroyo, "*Energy management strategy for a battery-diesel stand-alone system with distributed PV generation based on grid frequency modulation*", Journal of Renewable Energy, vol. 66, pp.325-336, 2014.
6. H. Jou, Y. Chang, J. Wu, K. Wu, "*Operation strategy for*

*a lab-scale grid-connected photovoltaic generation system integrated with battery energy storage*", Journal of Energy Conversion and Management, vol.89, pp.197–204, 2015.
7. P. Ruetschi, "*Aging mechanisms and service life of lead–acid batteries*", Journal of Power Sources, vol. 127, 33–44, 2004.
8. A. Bin, Y. Hongxing, H. Shen, L. Xianbo, "*Computer aided design for PV/Wind hybrid system*", Renew Energy, vol.28, pp.1491-512, 2003.
9. R. Yahmadi, K.Brik, F. Ben Ammar, "*Research of critical causes and improvement of energy storage system reliability in power electronic applications*", International journal of hydrogen energy, vol.42, pp. 8765-8776, 2016.
10. J.N. Ross, T. Markvart, "*Modelling Battery Charge Regulation for a Stand-alone Photovoltaic System*", Solar Energy, vol. 69, pp.181–190, 2000.
11. D. Parra, M. K. Patel, "*Effect of tariffs on the performance and economic benefits of PV-coupled battery systems*", Journal of Applied Energy, vol. 164, pp.175–187, 2016.
12. J. Doo-Hee, J. Sang-keun, R. Chung-Wook, H. Sung-Soo, H. Sang-Kyoo Han, "*High Power Density and Low Cost Photovoltaic Power Conditioning System with Energy Storage System*", IPEC, 2010 Conference Proceedings, IEEE.2010; pp.23 –240.
13. X. Liu, P. Wang, P. Loh, F. Gao, F.H. Choo, "*Control of Hybrid Battery/Ultra-capacitor Energy Storage for Stand-alone Photovoltaic System*", Journal of Energy Conversion Congress and Exposition (ECCE), IEEE 2010, 2010, pp.336-341.
14. J. Vaščák, "*Adaptation of fuzzy cognitive maps by migration algorithms*", Kybernetes, vol. 41, pp. 429-443, 2012.
15. R. Precup, M. Sabau, M. Petriub, "*Nature-inspired optimal tuning of input membership functions of Takagi-Sugeno-Kang fuzzy models for anti-lock braking systems* ", Applied Soft Computing, vol. 27, pp. 575-589, 2015.
16. Z. Ali, H. Awad, M. Duwairi, "*Multi-objective differential evolution algorithm with a new improved mutation strategy*", International Journal of Artificial Intelligence, vol. 14, pp. 23-41, 2016.
17. C. ZhimingChen, Z. Shaorui, L.Jieting, "*A robust ant colony optimization for continuous functions*", Expert Systems with Applications, vol. 81, pp. 309-320, 2017.
18. K. Nakanno, S. Takeshima, J. Furukawa, "*Technological Trends in Lead-Acid Batteries for Automotive Applications*", Furukawa Review, vol.32, pp.49-55, 2007.
19. N. Abd El-Shafy, "*An effective and safe charging algorithm for lead-acid batteries in PV systems*", International journal of energy research, vol. 35, pp.733–740, 2011.
20. M.A.S. Masoum, H. Dehbonei, E.F. Fuchs, "*Theoretical and experimental analyses of photovoltaic systems with voltage and current based maximum power-point tracking*", IEEE Trans. Energy Convers, vol.17, pp.514–522, 2002.
21. T. Esram, P.L. Chapman, "*Comparison of photovoltaic array maximum power point trackimg techniques*", IEEE Trans, Energy Convers, vol. 22, pp. 439–449, 2007.
22. A. Pradeep, K. Yadav, S. Thirumaliah, G. Haritha, "*Comparison of MPPT Algorithms for DC-DC Converters Based PV Systems*", International Journal of Advanced Research in Electrical, Electronics and Instrumentation Engineering, vol.1, pp.18-23, 2012.
23. T. Radjai, J. Gaubert, Q. Rahmani, S. Mekhilef, "*Experimental verification of P&O MPPT algorithm with direct control based on Fuzzy logic control using CUK converter*", International transactions on electrical energy systems, vol.25, pp. 3492–3508, 2015.
24. S. Mirbagheri, S. Mekhilef, S. Mohsen Mirhassani, "*MPPT with Inc.Cond method using conventional interleaved boost converter*", Energy Procedia, vol. 42, pp.24 – 32, 2013.
25. C. Armenta-Deu, "*Prediction of battery behaviour in SAPV Applications*", Renewable Energy, vol.28, pp.1671–1684, 2003.
26. K. Brik, F. Ben Ammar, "*Improved performance and energy management strategy for proton exchange membrane fuel cell/backup battery in power electronic systems*", International journal of hydrogen energy, vol.42, pp. 8845-8856, 2016.